Lithuanian Journal of Physics, Vol. **50**, No. 1, pp. 111–120 (2010) doi:10.3952/lithjphys.50101

# EFFICIENT 4-FOLD SELF-COMPRESSION OF MILLIJOULE PULSES FROM A 1.5-$\mu$m OPTICAL PARAMETRIC CHIRPED-PULSE AMPLIFIER

S. Ališauskas [a], V. Smilgevičius [a], A.P. Piskarskas [a], O.D. Mücke [b], A.J. Verhoef [b], A. Pugžlys [b], A. Baltuška [b], J. Pocius [a,c], L. Giniūnas [c], R. Danielius [c], and N. Forget [d]

[a] *Department of Quantum Electronics, Vilnius University, Saulėtekio 9, LT-10222 Vilnius, Lithuania*
E-mail: skirmantas.alisauskas@ff.vu.lt
[b] *Photonics Institute, Vienna University of Technology, Gusshausstr. 27-387, A-1040 Vienna, Austria*
[c] *Light Conversion Ltd., P/O Box 1485, Saulėtekio 10, LT-10223 Vilnius, Lithuania*
[d] *Fastlite, Bâtiment 403, Ecole Polytechnique, F-91128 Palaiseau, France*

Received 26 October 2009; revised 29 December 2009; accepted 19 March 2010

We discuss a four-stage optical parametric chirped-pulse amplifier that delivers carrier-envelope phase-stable $\sim$1.5 $\mu$m pulses with energies up to 12.5 mJ before recompression. The system (previously reported in Opt. Lett. **34**, 2498 (2009)) is based on a fusion of femtosecond diode-pumped solid-state Yb technology and a picosecond 100-mJ Nd:YAG pump amplifier. Pulses with 62 nm bandwidth are recompressed to a 74.4 fs duration, which is close to the transform limit. Here, to show the way towards a TW-peak-power single-cycle IR source, we perform detailed investigations of single-filament IR supercontinuum generation via femtosecond filamentation in noble gases. Depending on the experimental conditions, two filamentation regimes can be achieved: (i) in the filamentation regime without plasma-induced pulse self-compression, we generate 4-mJ 600-nm-wide IR supercontinua of high spatial quality supporting 8-fs pulse durations, which corresponds to less than two optical cycles at 1.5 $\mu$m; (ii) in the self-compression regime, we demonstrate self-compression of 2.2 mJ pulses down to 19.8 fs duration in a single filament in argon with a 1.5 mJ output energy and 66% energy throughput. By adapting the experimental conditions, further energy upscaling of the self-compressed pulses seems feasible.

**Keywords:** optical parametric amplification, filamentation, pulse self-compression, intense few-cycle infrared pulses

**PACS:** 42.65.Yj, 42.65.Re

## 1. Introduction

Optical parametric chirped-pulse amplification [1] (OPCPA) has attracted a lot of attention as a promising route towards intensity scaling of few-cycle laser pulses. Intense carrier-envelope phase (CEP)-stable few-cycle laser pulses have numerous intriguing applications in attosecond and high-field science including the production of attosecond XUV / soft-X-ray pulses by high-harmonic generation (HHG), tomographic imaging of molecular orbitals, and laser-induced electron diffraction (for a recent review, see [2]). A major challenge for using HHG in studies of time-resolved tomography of molecular dissociative states is the low ionization potential $I_\mathrm{p}$ of excited molecular states. The resulting competition between state depletion and HHG prevents generation of broad HHG spectra necessary for tomographic reconstruction. One solution are laser sources with high ponderomotive energy $U_\mathrm{p} \propto \lambda^2 I$ at moderate intensity level, i. e., IR CEP-stable few-cycle high-power laser systems. The present immense interest of the ultrafast community in high-$U_\mathrm{p}$ sources [3–11] has three major reasons:

1. These sources open the door to previously inaccessible regimes of light–matter interactions [12] and in particular they allow experimental investigations of the $\lambda$-scaling laws of strong-field physics [13–16] (Keldysh parameter $\propto \lambda^{-1}$, electron energies $\propto \lambda^2$, HHG cutoff $\propto \lambda^2$, minimum attosecond pulse duration $\propto \lambda^{1/2}$). In addition, e. g., laser-induced electron diffraction experiments [2] would benefit from IR driving because of the shorter de Broglie electron wavelength and consequently higher spatial resolution.
2. Because of the $\lambda^2$-dependence of the HHG cutoff [17–19], HHG driven by intense few-cycle IR sources holds great promise for the realization of


ISSN 1648-8504

bright coherent sources in the soft- and potentially even hard-X-ray region [20]. The achievable HHG photon fluence depends both on the microscopic single-atom response of the gas and on macroscopic effects in the gas target like phase matching and absorption. At present, both microscopic ($\lambda^{-(5-6)}$-scaling of the single-atom HHG conversion efficiency [13, 14, 21–23]) and macroscopic parts are subject of a heated scientific debate. Recent work on phase matching of higher harmonics driven by high-energy IR pulses [8, 9, 20, 24–26] indicate the feasibility to compensate the sharp drop of the microscopic HHG efficiency macroscopically by an increased optimal gas pressure for phase matching and the strongly decreasing reabsorption of the generated X-rays at higher photon energies.

3. The development of high-$U_\mathrm{p}$ sources is also of paramount importance for attosecond photoelectron spectroscopy of solid surfaces [27] and surface-adsorbate systems [28] because IR sources allow pronounced ponderomotive streaking effects already at lower laser intensity, thus avoiding background problems originating from above-threshold ionization or sample damage.

For many applications in attosecond science, in particular for the generation of isolated attosecond XUV / soft-X-ray pulses, extremely short pulses comprising only one or two light oscillations underneath the field envelope are required. Ultrabroadband near-degenerate Type I parametric amplification of CEP-stable two-cycle IR seed pulses obtained from difference-frequency generation (DFG) to the energy level close to 1 mJ has been demonstrated [3–7]. However, the inherently low DFG seed energy causes a sizable superfluorescence background [3, 4, 7] that prevents further energy upscaling. By narrowing the bandwidth of an optical parametric amplifier (OPA), one can optimize the spectral brightness of the seed at the expense of the seed energy, achieve a more uniform saturation across the pulse spectrum, and minimize energy backconversion into the pump. In saturation, however, the parametrically amplified spectra exhibit steep slopes that lead to poor fidelity of the compressed pulses in the time domain.

The well-established standard technology for the generation of few-cycle driver pulses is spectral broadening of mJ-level femtosecond pulses from Ti:sapphire amplifier systems in noble gases. Using 5-fs 1-mJ 720-nm driver pulses obtained in this way, coherent X-rays in the keV photon energy range were demonstrated by HHG in He [29]. At present, the energy throughput of gas-phase broadening schemes, such as the hollow-core fibre compressor [30, 31] and filamentation [32, 33], is limited to 4–5 mJ at 0.8 $\mu$m due to ionization losses [34, 35]. With multi-mJ pulses from an IR OPCPA we expect to ultimately surpass the present energy limitation for gas broadening schemes, since the critical power of self-focusing scales as $\lambda^2$ [36].

Here, we present a hybrid Type-II IR OPCPA / filamentation approach to pursue a TW-peak-power single-cycle IR source [10, 11] that will find many applications in attosecond and high-field science.

## 2. CEP-stable multimillijoule infrared OPCPA

The experimental chart of our four-stage IR OPCPA is depicted in Fig. 1. The front-end of the OPCPA is based on a femtosecond Yb:KGW diode-pumped solid-state (DPSS) master-oscillator power amplifier (MOPA) (Pharos, Light Conversion, Ltd.) and two stages of CEP-stable parametric preamplification [10]. Adding two OPCPA booster stages *3* and *4* allows us to reach pulse energies above 10 mJ. Following the pioneering work of Kraemer et al. [37, 38], we employ Type II phase-matching ($e_\mathrm{s} + o_\mathrm{i} \rightarrow o_\mathrm{p}$, $\theta = 45.5^\circ$, $\varphi = 0^\circ$) in $KTiOPO_4$ (KTP) crystals (1.03 $\mu$m / 1.064 $\mu$m pump, $\sim$1.5 $\mu$m signal, $\sim$3.3–3.7 $\mu$m idler) for OPA stages 2–4 because these crystals (unlike borate crystals) are transparent for the mid-IR idler wavelength and exhibit a relatively broad bandwidth around 1.5 $\mu$m. Moreover, Type-II OPA minimizes parasitic self-diffraction [39].

In our IR OPCPA scheme (see Fig. 1), both Yb:KGW and Nd:YAG regenerative amplifiers (RAs) are simultaneously seeded from a single Yb:KGW master oscillator that has a modest FWHM bandwidth of 30 nm centred at 1.04 $\mu$m (not shown). To seed the Nd:YAG RA, we pick up unused 1064-nm light behind a transmission grating in the pulse stretcher of the Yb:KGW MOPA. The repetition rate of this MOPA, tunable in the range of 1–100 kHz, was set at 10 kHz as the 500th harmonic of the flash-lamp-pumped Nd:YAG amplifier (Ekspla Ltd.) operating at 20 Hz. In the Nd:YAG RA, an intracavity etalon is used to narrow the pulse bandwidth and make the pulse duration (60 ps) safe for post-amplification.

In order to optimize the energy extraction from the 60 ps long Nd:YAG pump pulses, the passively CEP-stable 1.5-$\mu$m pulses from the front-end [10] are temporally stretched to $\sim$40 ps using a grating-based stretcher

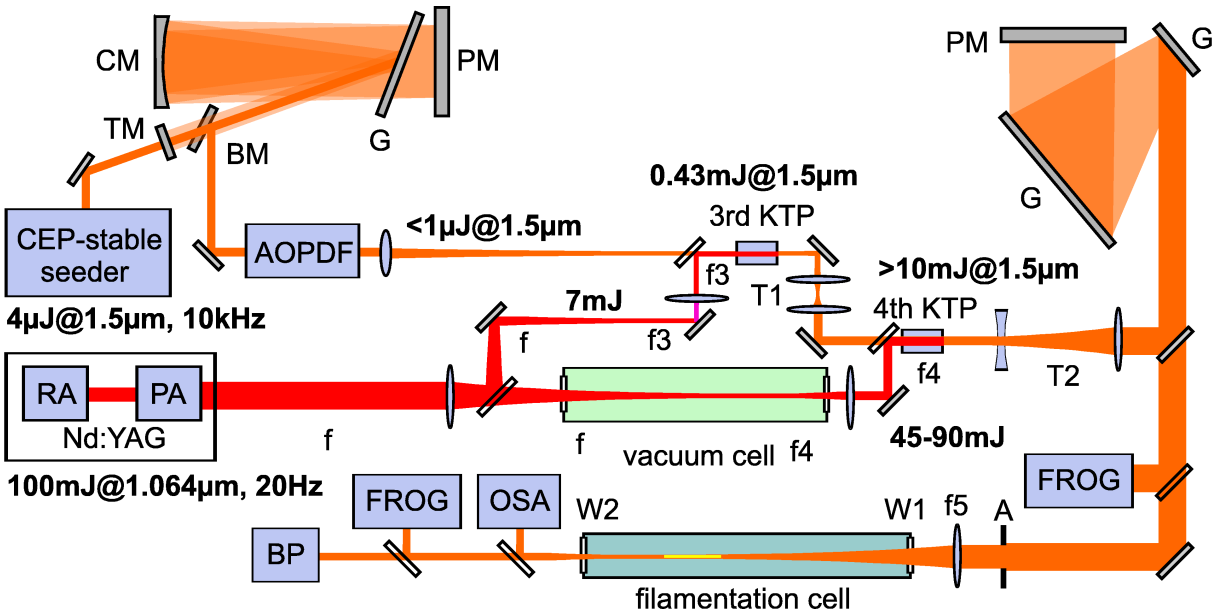


Fig. 1. Chart of the four-stage IR OPCPA and filamentation set-up: the CEP-stable seeder is the front-end described in [10]; *G*, reflection grating; *CM*, curved mirror; *PM*, plane mirror; *TM* / *BM*, top / bottom mirror; *AOPDF*, acousto-optic programmable dispersive filter; *RA*, regenerative amplifier; *PA*, double-pass post-amplifier; *f*, *f3*, *f4*, *f5*, lens focal lengths; *T1*, *T2*, telescopes; *A*, aperture; *W1* / *W2*, input / output windows; *OSA*, optical spectrum analyzer; *FROG*, frequency-resolved optical gating set-up; *BP*, beam profiler.

[40] employing 500 grooves/mm 96% efficient gold reflection gratings. In addition, an IR high-resolution acousto-optic programmable dispersive filter (DAZZLER) [41] is used for higher-order dispersion control. To guarantee a homogeneous pump profile free of hot spots, we relay-image the 10 mm diameter crystal rod in the Nd:YAG power amplifier onto the 10 mm thick KTP crystals in stages *3* and *4*. The measured surface damage threshold of KTP for our pump pulses (21 GW/cm$^2$) determines a pump spot diameter of 2 and 3.1 mm for stages *3* and *4*, respectively. Relay-imaging is achieved with three lenses with focal lengths of $f = 75$ cm, $f3 = 10$ cm, and $f4 = 35$ cm (see Fig. 1). Because of the larger pump intensities in the fourth OPA stage, the focus needs to be placed inside a vacuum cell to avoid a breakthrough in air. The 1.5-$\mu$m (seed) pulses [10] are focused onto the third-stage KTP crystal with a 750-mm lens and imaged onto the fourth-stage KTP crystal with telescope *T1*. The (external) walk-off compensation angle between the pump and seed beams is 2.2°. With this pumping geometry and ~90 mJ pump pulses, we have achieved up to 12.5 mJ signal pulses centred at 1.57 $\mu$m with a pump-signal conversion efficiency of ~22% in the final OPCPA stage. To avoid damage to the gold gratings in the OPCPA compressor, we expand the beam diameter of the fourth-stage output by a factor of 5 to 9.5 mm (at the $1/e^2$ level) by means of a Galilean beam expander *T2*.

The spectra of the seed and amplified signal pulses of the power-amplification stages are shown in Fig. 2. In principle, saturating the OPCPA stages permits amplification of pulses with nearly 80 nm bandwidth corresponding to a Fourier limit of ~65 fs. As idler absorption increases above 3.4 $\mu$m in KTP, we can achieve higher output powers when tuning the signal centre wavelength above 1.55 $\mu$m.

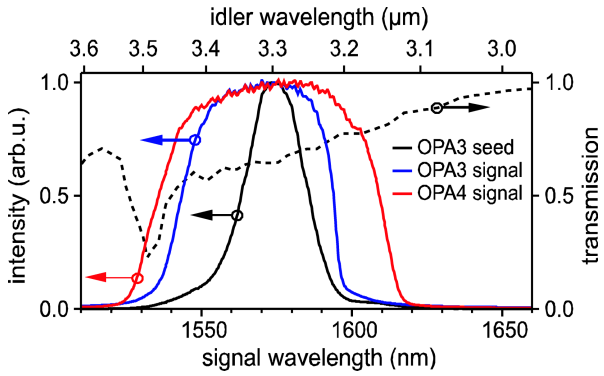


Fig. 2. Spectral properties of the booster-amplification OPCPA stages: spectrum of the third-stage seed (black curve), amplified signal spectra after stages *3* (blue online) and *4* (red online). The amount of superfluorescence is immeasurable in absence of the WL seed in OPA stage *1*. The dashed curve indicates the idler transmission through 10 mm of KTP.

The SHG-frequency-resolved optical gating (FROG) data of 3.5-mJ 1.57-$\mu$m pulses with 62-nm bandwidth from the 20-Hz four-stage IR OPCPA (see Fig. 3) indicate a 74.4-fs FWHM pulse duration, close to the transform limit (TL) of 72.6 fs. Ultimately, with further

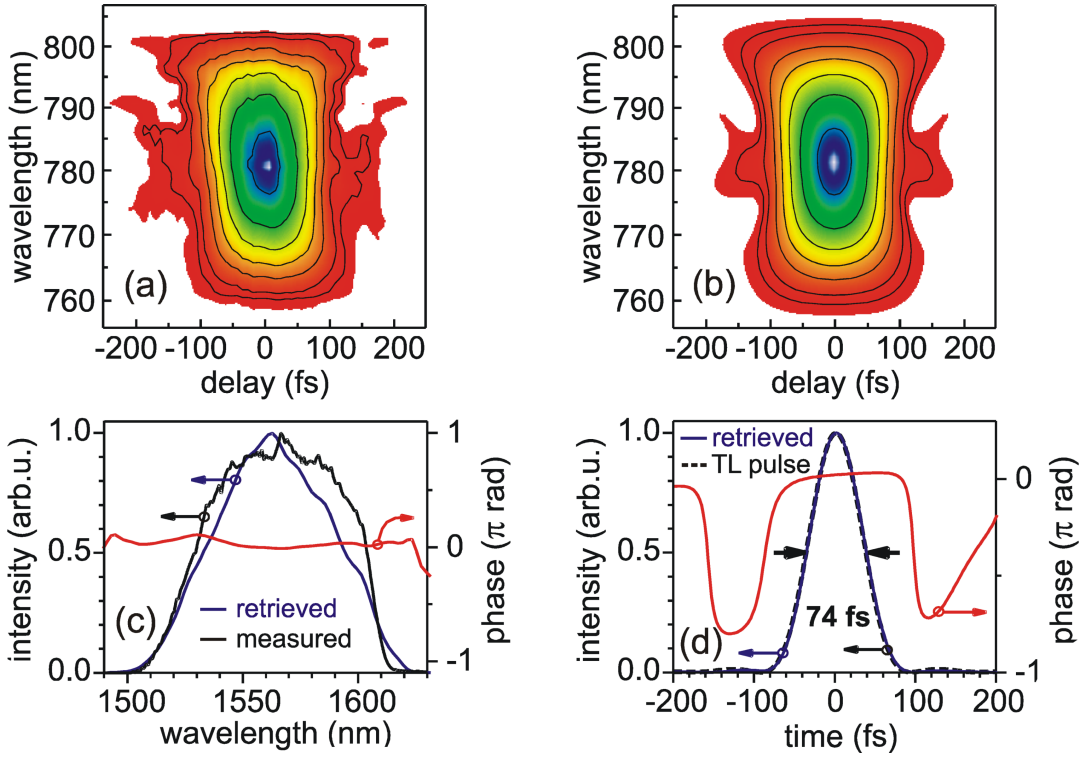


Fig. 3. SHG-FROG characterization of the 20-Hz output from the four-stage IR OPCPA: (a) measured and (b) retrieved FROG traces. (c) Measured spectrum (black curve), retrieved spectral intensity (blue online) and phase (red online). (d) Retrieved temporal intensity (blue online) and phase (red online) profiles exhibiting a 74.4-fs FWHM pulse duration. The TL intensity profile (dashed) corresponds to a 72.6-fs duration.

optimization sub-70-fs pulse durations seem in reach by recompressing pulses with bandwidths approaching 80 nm.

## 3. Spectral broadening and pulse self-compression via filamentation in noble gases

In the following, we demonstrate single-filament IR supercontinuum generation via femtosecond filamentation in noble gases. Depending on the experimental conditions, two filamentation regimes can be achieved: (i) the filamentation regime without plasma-induced pulse self-compression, as discussed in Sec. 3.1, and (ii) the self-compression regime, as discussed in Sec. 3.2. Ultimately, since the critical power of self-focusing scales as $\lambda^2$ [36], we expect to surpass the current energy limitation (4–5 mJ at 800 nm [34, 35]) with the multi-mJ femtosecond pulses obtained from our IR OPCPA. In addition, a promising route for further pulse energy upscaling is the use of circularly / elliptically polarized input pulses [42, 43].

### *3.1. Multimillijoule IR filamentation without plasma-induced pulse self-compression*

In the filamentation experiments (see Fig. 1), the 1.57-$\mu$m OPCPA pulses were focused using a 50-cm lens placed 4 cm in front of the anti-reflection-coated input window *W1* of a 138 cm long gas cell filled with argon ($I_p$ = 15.76 eV) or krypton ($I_p$ = 13.99 eV) at the absolute pressure of 4–5 bar. In the filamentation regime without plasma-induced pulse self-compression (Fig. 4), we generated ~3-mJ 600 nm wide IR supercontinua of high spatial quality supporting 8-fs pulse durations, which corresponds to less than two optical cycles at 1.5 $\mu$m.

SHG-FROG data of such spectrally broadened pulses are displayed in Fig. 5. We emphasize that the FROG characterization (Figs. 5 and 6) and corresponding output pulse energy measurements were performed without aperturing the filamentation output beam. In the experiment shown in Fig. 5, the input pulse energy was 3.0 mJ, output energy 2.1 mJ, corresponding to an energy throughput of 68% including the 8% reflection losses on the uncoated 1 mm thick BK7 output window *W2* (see Fig. 1). The SHG-FROG data reveal a rather complex spectro-temporal structure. The ob-

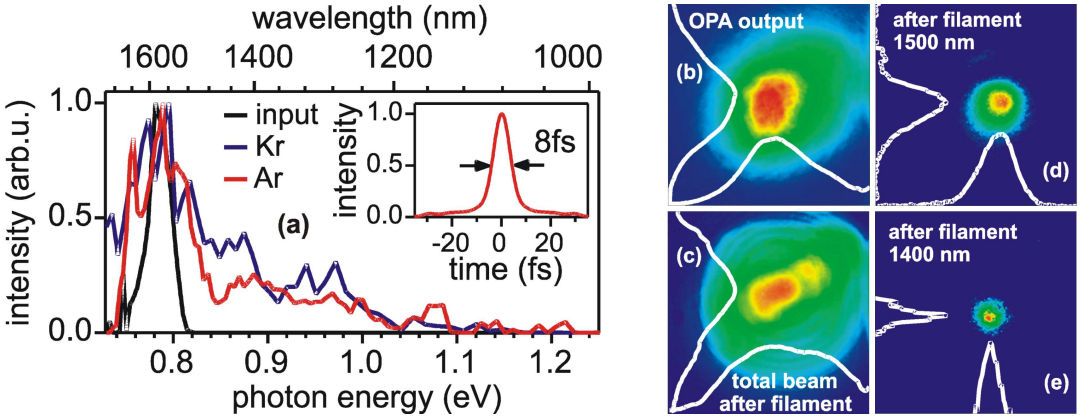


Fig. 4. (a) Filamentation of 1.57-$\mu$m pulses in noble gases: individually normalized input (black curve) and output spectra for filamentation of 0.8-mJ pulses in krypton (blue online) and 2.5-mJ pulses in argon (red online) at a 5 bar pressure. The inset shows the TL intensity profile computed from the argon output spectrum. (b)–(e) Far-field spatial beam profiles measured with a pyroelectric 2D array: (b) before the OPCPA grating compressor; (c) total (frequency-unresolved) beam profile behind the Ar cell; (d) beam profile at 1500 nm; (e) beam profile at 1400 nm. (d) and (e) are taken at the same camera position as (c) by inserting narrow-band filters into the beam. Image size is $12.4\times12.4$ mm$^2$.

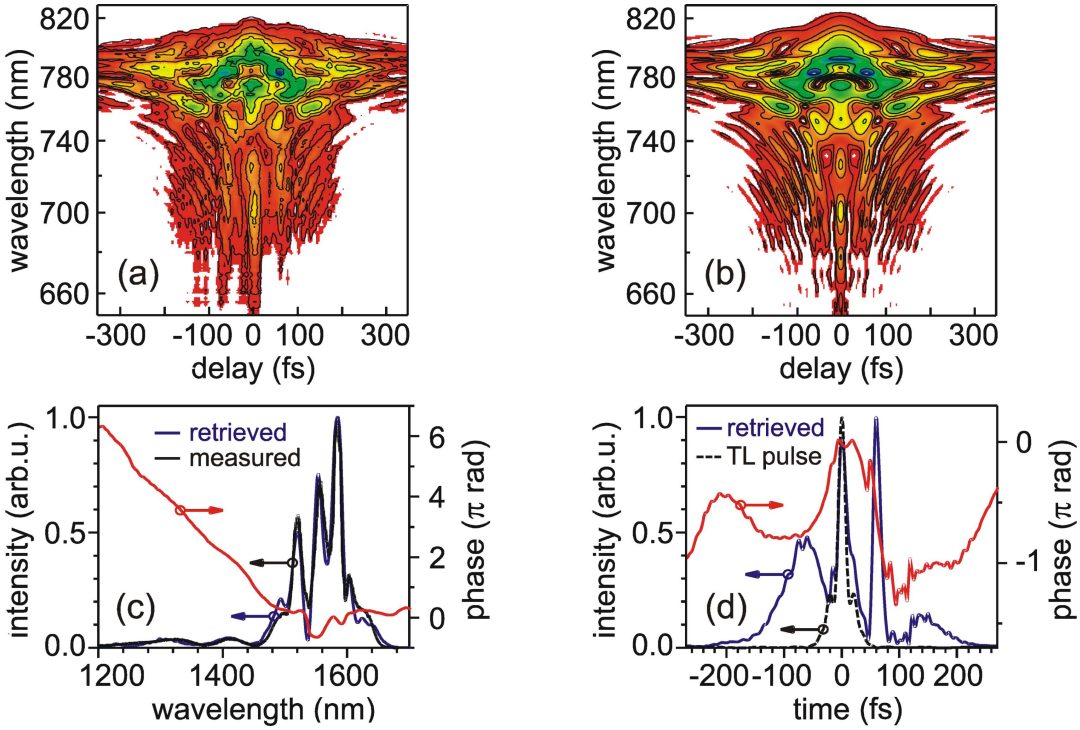


Fig. 5. SHG-FROG characterization of 2.1-mJ filamentation output pulses for argon at 4 bar: (a)–(d) as in Fig. 3. The TL intensity profile (dashed) corresponds to a 14.6-fs duration.

served strong nonlinear phase leads to a temporal break-up into two peaks of 20 fs and 15 fs FWHM duration, separated by 60 fs. Since a clean single-filament spatial profile was observed simultaneously, we conclude that the temporal splitting apparently helps to keep the pulse intensity below the break-up threshold of a single filament.

### *3.2. Self-compression of millijoule IR pulses*

The filamentation regime involving plasma-induced pulse self-compression is particularly attractive for the pursuit of a TW-peak-power single-cycle IR source. Recently, Hauri et al. [33] demonstrated that filamentation of rather long ~55-fs OPA pulses at 2 $\mu$m in

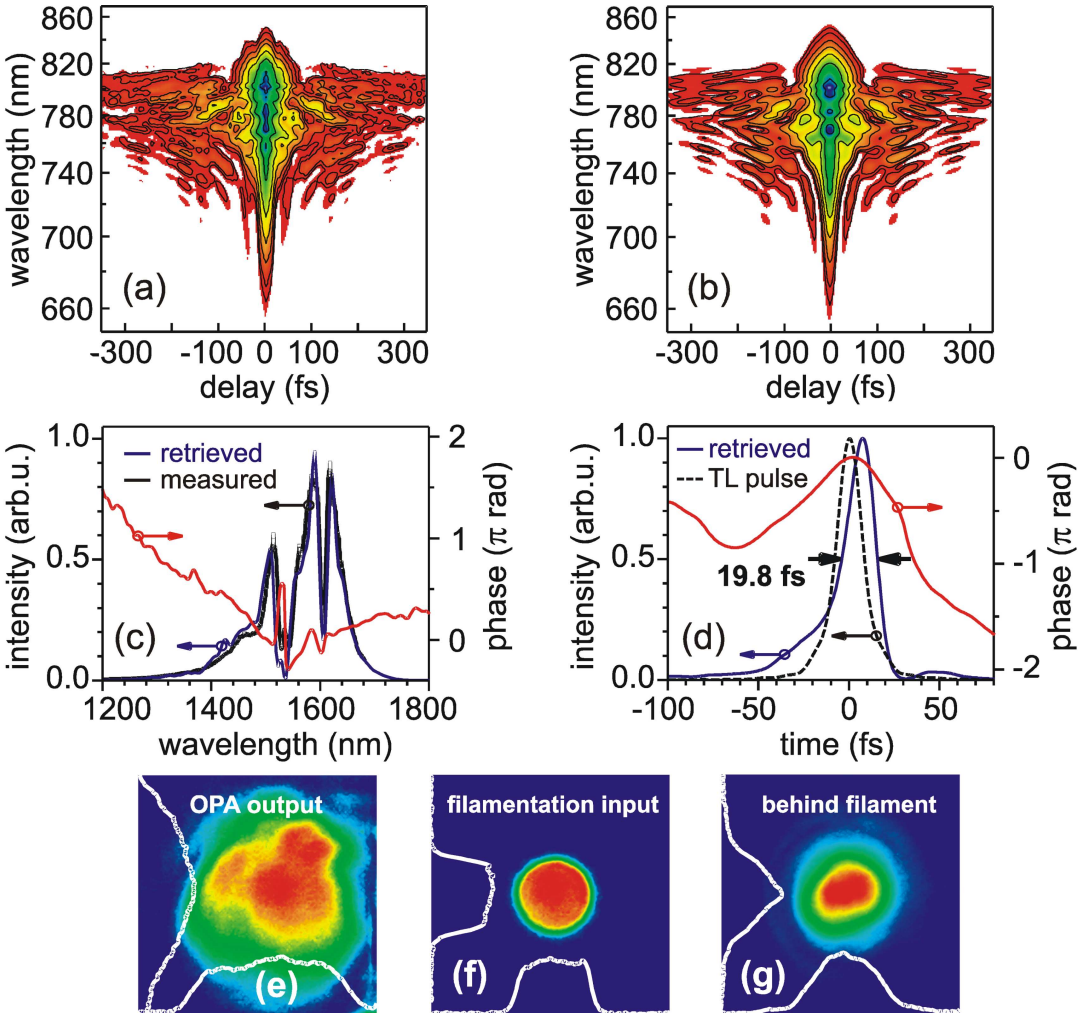


Fig. 6. Self-compression of 1.5-mJ pulses in argon at 5 bar: (a)–(d) as in Fig. 3. The retrieved FWHM pulse duration is 19.8 fs, 15.9 fs Fourier limit. (e)–(g) Far-field spatial beam profiles measured with the pyroelectric 2D array: (e) after OPCPA grating compressor; (f) apertured filamentation input behind the iris aperture $A$; (g) total beam profile behind the filamentation cell. Image size is $12.4\times12.4$ mm$^2$.

a xenon cell allows the generation of self-compressed 17-fs 0.27-mJ pulses. The limited input pulse energy available in that experiment implied the use of xenon as a noble gas with the highest nonlinearity. Detailed numerical investigation of self-compression of 2-$\mu$m laser filaments [36] predicted a number of highly attractive features of femtosecond filamentation at longer carrier wavelength $\lambda$: (i) the bandwidth of the generated supercontinuum increases with $\lambda$; (ii) for comparable ratios of input power over critical power, $P_{\rm in}/P_{\rm crit}$, filaments at IR wavelengths have higher pulse energy than near-VIS filaments; (iii) the filament channel extends over longer distances and its waist scales $\propto \lambda$; (iv) self-steepening becomes more pronounced with increasing $\lambda$; (v) for gases with moderate ionization potentials ($I_{\rm p} < 20$ eV, e. g., argon or xenon), the numerical calculations reveal that mid-IR filamentation easily permits self-compression to single-cycle pulse durations, as compared to self-compressed 2–3 cycle durations at visible wavelengths. Self-compression of 2-$\mu$m pulses results in supercontinua exhibiting a much flatter spectral phase over the full bandwidth as compared to 800-nm pulses. Bergé [36] also made the important observation that for self-compression of 2-$\mu$m pulses, due to nonlinear pulse propagation the shortest achievable pulse duration survives only over shorter distances (∼15–20 cm) in the gas medium as compared to the 800-nm case (∼60 cm), i. e., the proper choice of the output window position with respect to the filament channel is crucial for observing optimum self-compression.

By lowering the input pulse energy using the iris aperture $A$ and tuning the gas pressure in the cell, we achieved the regime of pulse self-compression. In the experiment shown in Fig. 6, CEP-stable 2.2-mJ 74.4-fs 1.57-$\mu$m input pulses are compressed in a single

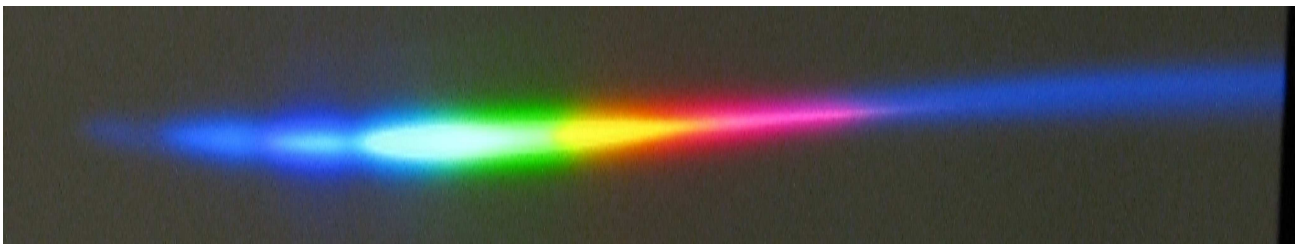

Fig. 7. Photo of the spectrally resolved filamentation output in the self-compression regime.

filament in argon down to a 19.8-fs duration. This represents a temporal compression of the input pulses by a factor of ∼4. The output energy was 1.5 mJ, corresponding to an energy throughput of 66%, again including the 8% reflection losses on window *W2*. The IR supercontinuum with a 130-nm FWHM bandwidth originates from a 12–15 cm long filament. The low-intensity spectral wings of the supercontinuum extend throughout the VIS and are easily visible with the naked eye (see Fig. 7). As argued above, careful optimization of the propagation distance in the pressurized Ar cell behind the filament might lead to the observation of even shorter pulse durations [36]. In addition, the spectral phase is remarkably reproducible on a daily basis which holds potential for further recompression using fixed-dispersion chirped mirrors.

Concerning the CEP stability of the filamentation output, several femtosecond filamentation experiments performed at various centre wavelengths [32, 33] have clearly demonstrated that the filamentation process preserves the CEP stability of the input pulses. Therefore, we are convinced that the filamentation process does not degrade the CEP stability of the OPCPA input pulses in our experiment. Nevertheless, in order to quantify the quality of CEP stability, we are planning (i) to perform inline $f$-to-$2f$ interferometry to the OPCPA output of stages *3* and *4*, (ii) quantify possible differential CEP drifts caused in the individual amplification stages *3* and *4* using a TADPOLE-type technique [44], (iii) and finally perform $f$-to-$3f$ interferometry (since a sizable third harmonic is generated inside the filament) to the filamentation output.

### *3.3. Time–frequency analysis employing Wigner distribution functions*

For the time–frequency analysis, it is very instructive to look at the Wigner distributions [45]

$$W(t,\omega) = \int \mathrm{d}\tau\, E^*\left(t-\frac{\tau}{2}\right) E\left(t+\frac{\tau}{2}\right) \exp(\mathrm{i}\omega\tau) \tag{1}$$

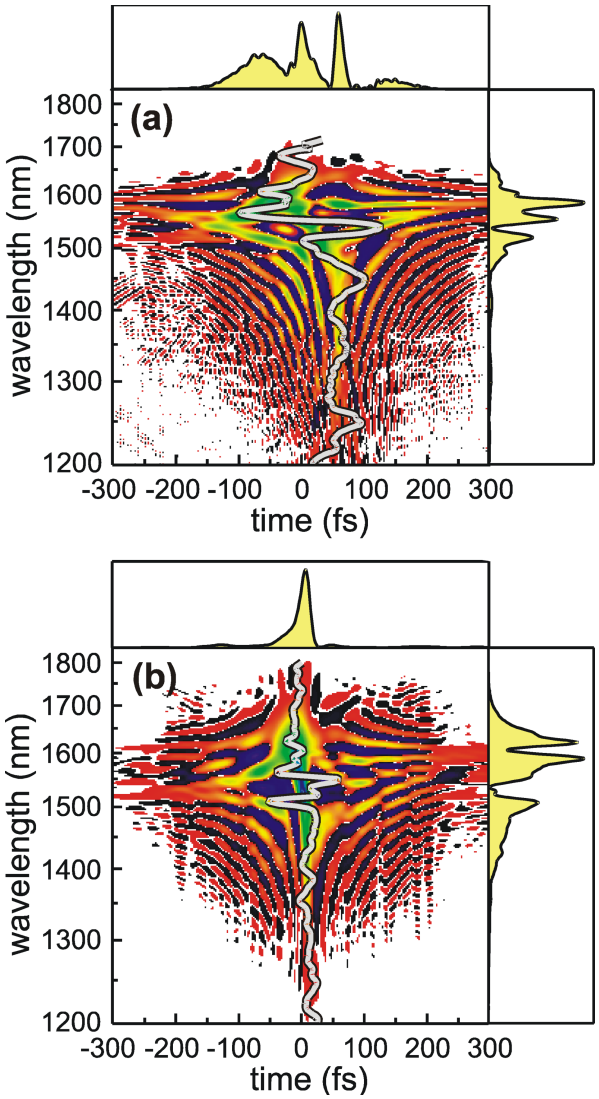


Fig. 8. Wigner distribution functions: (a) filamentation without self-compression extracted from the SHG-FROG data in Fig. 5, (b) self-compression result obtained from Fig. 6. The grey curves indicate the retrieved group delay (GD). The panels above and on the right indicate the temporal intensity profile and pulse spectrum, respectively.

directly computed from the FROG data. When integrating these 2D data over wavelength, one obtains the

temporal intensity profile, while integration over time yields the pulse spectrum:

$$I(t) = \int \mathrm{d}\omega\, W(t,\omega) \quad \text{and} \quad \tilde{I}(\omega) = \int \mathrm{d}t\, W(t,\omega)\,. \tag{2}$$

The Wigner distribution functions extracted from the filamentation FROG data corresponding to the two distinct filamentation regimes are displayed in Fig. 8. Although the SHG-FROG traces in Figs. 5 and 6 look qualitatively rather different, the Wigner distributions now look more similar. The main difference is that in the self-compression regime (Fig. 8(b)), the group delay is much flatter and exhibits much smaller oscillations than the data obtained in the filamentation regime without self-compression (Fig. 8(a)). The fact that both cases do not differ qualitatively gives us hope that, by adapting the experimental conditions, it should be possible to achieve self-compression of multi-mJ 1.6 $\mu$m pulses in the future.

## 4. Conclusions and outlook

In conclusion, we have discussed CEP-stable parametric amplification at 1.5 $\mu$m signal wavelength with pulse energies up to 12.5 mJ based on a fusion of a DPSS femtosecond Yb:KGW MOPA system and picosecond Nd:YAG solid-state technology. To show the way towards a TW-peak-power single-cycle IR source, we performed detailed investigations of single-filament IR supercontinuum generation via femtosecond filamentation in noble gases. Namely, in the filamentation regime without plasma-induced pulse self-compression, we generated 4-mJ 600-nm-wide IR supercontinua of high spatial quality supporting 8-fs pulse durations, which corresponds to less than two optical cycles at 1.5 $\mu$m. In the self-compression regime, we demonstrated self-compression of CEP-stable 2.2-mJ 74.4-fs 1.57-$\mu$m input pulses down to 19.8 fs duration in a single filament in argon with a 1.5 mJ output energy and 66% energy throughput. The output energy was scaled up by 5.6 times over earlier results [33]. The output energy and energy throughput can be further increased by systematically optimizing the experimental conditions (input pulse energy and beam diameter, focusing lens and position, gas type and pressure, input polarization, gas cell length, etc.). At present, the pulse energy limit for gas broadening schemes is 4–5 mJ at 800 nm [34, 35]. Theoretical investigations by Bergé [36] predicted a number of attractive features of femtosecond filamentation at longer wavelengths including higher filament energies, broader supercontinua with a flatter spectral phase, and the feasibility to reach single-cycle pulse durations in comparison with 2–3-cycle durations at visible wavelengths. Moreover, a time–frequency analysis of our filamentation data employing Wigner distribution functions suggests that, by adapting the experimental conditions (e. g., input pulse energy and input iris aperture $A$, focusing conditions), the self-compression regime can also be reached at higher multi-mJ pulse energies. For these reasons, with 1.6-$\mu$m pulses we ultimately expect to surpass the present energy limitation (4–5 mJ at 800 nm) for gas broadening schemes.

## Acknowledgements

This work has been supported by the Austrian Science Fund (FWF), grants U33-N16 and F1619-N08, LASERLAB-EUROPE II (JRA HAPPIE), and partly supported by the Lithuanian State Science and Studies Foundation (project No. B-42/2009). ODM gratefully acknowledges support from a Lise-Meitner Fellowship by the FWF (project M1094-N14).

## References

[1] A. Dubietis, R. Butkus, and A.P. Piskarskas, IEEE J. Sel. Top. Quant. Electron. **12**, 163–172 (2006).

[2] F. Krausz and M. Ivanov, Rev. Mod. Phys. **81**, 163–234 (2009).

[3] T. Fuji, N. Ishii, C.Y. Teisset, X. Gu, T. Metzger, A. Baltuška, N. Forget, D. Kaplan, A. Galvanauskas, and F. Krausz, Opt. Lett. **31**, 1103–1105 (2006).

[4] X. Gu, G. Marcus, Y. Deng, T. Metzger, C. Teisset, N. Ishii, T. Fuji, A. Baltuska, R. Butkus, V. Pervak, H. Ishizuki, T. Taira, T. Kobayashi, R. Kienberger, and F. Krausz, Opt. Express **17**, 62–69 (2009).

[5] C. Vozzi, G. Cirmi, C. Manzoni, E. Benedetti, F. Calegari, G. Sansone, S. Stagira, O. Svelto, S. De Silvestri, M. Nisoli, and G. Cerullo, Opt. Express **14**, 10109–10116 (2006).

[6] C. Vozzi, F. Calegari, E. Benedetti, S. Gasilov, G. Sansone, G. Cerullo, M. Nisoli, S. De Silvestri, and S. Stagira, Opt. Lett. **32**, 2957–2959 (2007).

[7] J. Moses, S.-W. Huang, K.-H. Hong, O.D. Mücke, E.L. Falcão-Filho, A. Benedick, F.Ö. Ilday, A. Dergachev, J.A. Bolger, B.J. Eggleton, and F.X. Kärtner, Opt. Lett. **34**, 1639–1641 (2009).

[8] E.J. Takahashi, T. Kanai, Y. Nabekawa, and K. Midorikawa, Appl. Phys. Lett. **93**, 041111-1–3 (2008).

[9] E.J. Takahashi, T. Kanai, K.L. Ishikawa, Y. Nabekawa, and K. Midorikawa, Phys. Rev. Lett. **101**, 253901-1–4 (2008).

[10] O.D. Mücke, D. Sidorov, P. Dombi, A. Pugžlys, A. Baltuška, S. Ališauskas, V. Smilgevičius, J. Pocius, L. Giniūnas, R. Danielius, and N. Forget, Opt. Lett. **34**, 118–120 (2009).

[11] O.D. Mücke, S. Ališauskas, A.J. Verhoef, A. Pugžlys, A. Baltuška, V. Smilgevičius, J. Pocius, L. Giniūnas, R. Danielius, and N. Forget, Opt. Lett. **34**, 2498–2500 (2009).

[12] C.I. Blaga, F. Catoire, P. Colosimo, G.G. Paulus, H.G. Muller, P. Agostini, and L.F. DiMauro, Nature Phys. **5**, 335–338 (2009).

[13] J. Tate, T. Auguste, H.G. Muller, P. Salières, P. Agostini, and L.F. DiMauro, Phys. Rev. Lett. **98**, 013901-1–4 (2007).

[14] P. Colosimo, G. Doumy, C.I. Blaga, J. Wheeler, C. Hauri, F. Catoire, J. Tate, R. Chirla, A.M. March, G.G. Paulus, H.G. Muller, P. Agostini, and L.F. DiMauro, Nature Phys. **4**, 386–389 (2008).

[15] G. Doumy, J. Wheeler, C. Roedig, R. Chirla, P. Agostini, and L.F. DiMauro, Phys. Rev. Lett. **102**, 093002-1–4 (2009).

[16] P. Agostini and L.F. DiMauro, Contemp. Phys. **49**, 179–197 (2008).

[17] B. Sheehy, J.D.D. Martin, L.F. DiMauro, P. Agostini, K.J. Schafer, M.B. Gaarde, and K.C. Kulander, Phys. Rev. Lett. **83**, 5270–5273 (1999).

[18] B. Shan and Z. Chang, Phys. Rev. A **65**, 011804(R)-1–4 (2001).

[19] A. Gordon and F.X. Kärtner, Opt. Express **13**, 2941–2947 (2005).

[20] T. Popmintchev, M.-C. Chen, A. Bahabad, M. Gerrity, P. Sidorenko, O. Cohen, I.P. Christov, M.M. Murnane, and H.C. Kapteyn, Proc. Natl. Acad. Sci. USA **106**, 10516–10521 (2009).

[21] K. Schiessl, K.L. Ishikawa, E. Persson, and J. Burgdörfer, Phys. Rev. Lett. **99**, 253903-1–4 (2007).

[22] A.D. Shiner, C. Trallero-Herrero, N. Kajumba, H.-C. Bandulet, D. Comtois, F. Légaré, M. Giguère, J.-C. Kieffer, P.B. Corkum, and D.M. Villeneuve, Phys. Rev. Lett. **103**, 073902-1–4 (2009).

[23] M.V. Frolov, N.L. Manakov, T.S. Sarantseva, M.Y. Emelin, M.Y. Ryabikin, and A.F. Starace, Phys. Rev. Lett. **102**, 243901-1–4 (2009).

[24] T. Popmintchev, M.-C. Chen, O. Cohen, M.E. Grisham, J.J. Rocca, M.M. Murnane, and H.C. Kapteyn, Opt. Lett. **33**, 2128–2130 (2008).

[25] V.S. Yakovlev, M. Ivanov, and F. Krausz, Opt. Express **15**, 15351–15364 (2007).

[26] E.L. Falcão-Filho, V.M. Gkortsas, A. Gordon, and F.X. Kärtner, Opt. Express **17**, 11217–11229 (2009).

[27] A.L. Cavalieri, N. Müller, T. Uphues, V.S. Yakovlev, A. Baltuška, B. Horvath, B. Schmidt, L. Blümel, R. Holzwarth, S. Hendel, M. Drescher, U. Kleineberg, P.M. Echenique, R. Kienberger, F. Krausz, and U. Heinzmann, Nature **449**, 1029–1032 (2007).

[28] L. Miaja-Avila, G. Saathoff, S. Mathias, J. Yin, C. Lao-vorakiat, M. Bauer, M. Aeschlimann, M.M. Murnane, and H.C. Kapteyn, Phys. Rev. Lett. **101**, 046101-1–4 (2008).

[29] J. Seres, E. Seres, A.J. Verhoef, G. Tempea, C. Streli, P. Wobrauschek, V. Yakovlev, A. Scrinzi, C. Spielmann, and F. Krausz, Nature **433**, 596 (2005).

[30] M. Nisoli, S. De Silvestri, and O. Svelto, Appl. Phys. Lett. **68**, 2793–2795 (1996).

[31] M. Nisoli, S. De Silvestri, O. Svelto, R. Szipöcs, K. Ferencz, C. Spielmann, S. Sartania, and F. Krausz, Opt. Lett. **22**, 522–524 (1997).

[32] C.P. Hauri, W. Kornelis, F.W. Helbing, A. Heinrich, A. Couairon, A. Mysyrowicz, J. Biegert, and U. Keller, Appl. Phys. B **79**, 673–677 (2004).

[33] C.P. Hauri, R.B. Lopez-Martens, C.I. Blaga, K.D. Schultz, J. Cryan, R. Chirla, P. Colosimo, G. Doumy, A.M. March, C. Roedig, E. Sistrunk, J. Tate, J. Wheeler, L.F. DiMauro, and E.P. Power, Opt. Lett. **32**, 868–870 (2007).

[34] A. Suda, M. Hatayama, K. Nagasaka, and K. Midorikawa, Appl. Phys. Lett. **86**, 111116-1–3 (2005).

[35] G. Stibenz, N. Zhavoronkov, and G. Steinmeyer, Opt. Lett. **31**, 274–276 (2006).

[36] L. Bergé, Opt. Express **16**, 21529–21543 (2008).

[37] D. Kraemer, R. Hua, M.L. Cowan, K. Franjic, and R.J.D. Miller, Opt. Lett. **31**, 981–983 (2006).

[38] D. Kraemer, M.L. Cowan, R. Hua, K. Franjic, and R.J.D. Miller, J. Opt. Soc. Am. B **24**, 813–818 (2007).

[39] A. Varanavičius, A. Dubietis, A. Beržanskis, R. Danielius, and A. Piskarskas, Opt. Lett. **22**, 1603–1605 (1997).

[40] M.P. Kalashnikov, E. Risse, H. Schönnagel, and W. Sandner, Opt. Lett. **30**, 923–925 (2005).

[41] F. Verluise, V. Laude, J.-P. Huignard, P. Tournois, and A. Migus, J. Opt. Soc. Am. B **17**, 138–145 (2000).

[42] A. Trisorio and C.P. Hauri, Opt. Lett. **32**, 1650–1652 (2007).

[43] O. Varela, A. Zaïr, J. San Román, B. Alonso, I.J. Sola, C. Prieto, and L. Roso, Opt. Express **17**, 3630–3639 (2009).

[44] D.N. Fittinghoff, J.L. Bowie, J.N. Sweetser, R.T. Jennings, M.A. Krumbügel, K.W. DeLong, R. Trebino, and I.A. Walmsley, Opt. Lett. **21**, 884–886 (1996).

[45] J. Paye, IEEE J. Quantum Electron. **28**, 2262–2273 (1992).

# FAZIŠKAI MODULIUOTŲ MILIDŽAULINĖS ENERGIJOS IMPULSŲ PARAMETRINIS STIPRINTUVAS 1,5 $\mu$m SRITYJE SU IMPULSŲ SAVISPŪDA INERTINĖSE DUJOSE

S. Ališauskas [a], V. Smilgevičius [a], A.P. Piskarskas [a], O.D. Mücke [b], A.J. Verhoef [b], A. Pugžlys [b], A. Baltuška [b], J. Pocius [a,c], L. Giniūnas [c], R. Danielius [c], N. Forget [d]

[a] *Vilniaus universitetas, Vilnius, Lietuva*
[b] *Vienos technologijos universiteto Fotonikos institutas, Viena, Austrija*
[c] *UAB „Šviesos konversija“, Vilnius, Lietuva*
[d] *Fastlite, Palaiseau, Prancūzija*

**Santrauka**

Pademonstruotas stabilizuotos fazės keturių pakopų II fazinio sinchronizmo tipo faziškai moduliuotų impulsų parametrinis stiprintuvas 1,5 $\mu$m srityje. Jo impulso energija prieš kompresiją siekia 12,5 mJ. Parametrinio stiprintuvo sistema sudaryta iš femtosekundinio diodais kaupinamo Yb:KGV ir pikosekundinio lempomis kaupinamo 100 mJ Nd:IAG lazerių. Parametriškai sustiprinti impulsai, kurių spektro plotis pusaukštyje siekia 62 nm, buvo suspausti iki 74,4 fs, t. y. beveik iki spektriškai riboto impulso. Norint atskleisti galimybę generuoti kelių ciklų trukmės TW eilės smailinės galios impulsus IR srityje, buvo sugeneruotas 4 mJ 600 nm spektro pločio filamentas, kuris atitiktų 8 fs spektriškai ribotą impulsą. Taip pat argono dujose pademonstruota 2,2 mJ energijos impulso filamentacija su savispūda iki 19,8 fs pavienėje gijoje, 66% energijos pralaidumu ir siekianti 1,5 mJ energiją išvade.